EUROfusion

EUROFUSION WPDIV–PR(15)02

J.H. You et al.

Copper Matrix Composites as Heat Sink Materials for Water-Cooled Divertor Target

Preprint of Paper to be submitted for publication in
Nuclear Materials and Energy

This work has been carried out within the framework of the EUROfusion Consortium and has received funding from the Euratom research and training programme 2014-2018 under grant agreement No 633053. The views and opinions expressed herein do not necessarily reflect those of the European Commission.

Copper matrix composites as heat sink materials for water-cooled divertor target

Jeong-Ha You*

Max Planck Institute for Plasma Physics, Boltzmann Str. 2, 85748 Garching, Germany

*Contact
e-mail: you@ipp.mpg.de
Phone: ++49 (0)89 3299 1373
Fax: ++49 (0)89 3299 1212

Abstract

According to the recent HHF qualification tests of ITER divertor target mock-ups and the preliminary design studies of DEMO divertor target, the performance of CuCrZr alloy, the baseline heat sink material for DEMO divertor, seems to only marginally cover the envisaged operation regime. The structural integrity of the CuCrZr heat sink was shown to be affected by plastic fatigue at 20 MW/m². The relatively high neutron irradiation dose expected for the DEMO divertor target is another serious concern, as it would cause significant embrittlement below 250 °C or irradiation creep above 350 °C. Hence, an advanced design concept of target needs to be devised for DEMO in order to enhance the HHF performance so that the structural design criteria are fulfilled for full operation scenarios including slow transients. The biggest potential lies in copper-matrix composite materials for the heat sink. In this review article, three promising Cu-matrix composite materials are reviewed in terms of thermal, mechanical and HHF performance as structural heat sink materials. The considered candidates are W particle-reinforced, W wire-reinforced and SiC fiber-reinforced Cu matrix composites. The comprehensive results of recent studies on fabrication technology, design concepts, materials properties and the HHF performance of mock-ups are presented. Limitations and challenges are discussed.

Keywords: DEMO, divertor target, high-heat-flux loads, heat sink, composite materials, strength

1. Introduction

Precipitation-hardened CuCrZr alloy has been the most favored heat sink material used for the plasma-facing components (PFCs) of major fusion devices [1-4]. Currently, CuCrZr alloy is also considered as baseline heat sink material for the water-cooled divertor target of DEMO reactors [5]. The main benefit of using CuCrZr alloy as heat sink material for high-heat-flux (HHF) applications lies in the fact that it offers unique combination of desired properties, namely, excellent thermal conductivity, strength at operation temperature, ductility, toughness, machinability, water-tightness, and only moderate activation. It is noted that the heat sink of a PFC is supposed to assume structural function. This means that CuCrZr alloy shall be used as structural material for the PFC.

However, in spite of the extraordinary virtues listed above, the harsh loading environment expected for the PFCs of future fusion reactors (e.g. DEMO) will be highly challenging for CuCrZr alloy as heat sink material. For instance, the divertor target plate of a DEMO reactor shall be subjected to severe HHF loads on their surface which is expected to range, similarly to ITER, from 1 to 10 MW/m² during stationary operation and even up to 20 MW/m² in slow transient events [5, 6]. The HHF fatigue qualification tests conducted on ITER divertor target mock-ups showed that the CuCrZr heat sink tube as well as the tungsten armor block could be visibly damaged at the limit heat flux load of 20 MW/m² [1].

Furthermore, irradiation of fast neutrons is another critical issue. It causes degradation of thermal and mechanical properties of materials. Embrittlement due to lattice damage is the most negative consequence of irradiation which raises a critical design issue in terms of structural reliability. In the case of DEMO, the irradiation dose rate on the divertor target (W, Cu) is estimated to range between 3 and 10 dpa per full power year (fpy), which is high enough to cause pronounced embrittlement in the CuCrZr heat sink [7, 8].

In the following we focus our discussion on the heat sink of diverter target, an in-vessel PFC to be exposed to the highest heat flux loads in a reactor. Given that the heat sink of a divertor target has to withstand both cyclic HHF loads and neutron irradiation to a significant extent, maintaining a superior heat conductivity and sufficient mechanical stability at the predicted neutron dose is the paramount requirement for heat sink material. In addition, flexibility in the allowable operation temperature range is desired. In general, increased operation temperature leads to thermal softening and irradiation creep whereas the lowering of temperature enhances irradiation embrittlement [9].

In this context, there is a concern whether a CuCrZr-based heat sink can fulfill the structural design criteria formulated for DEMO divertor targets. This question is primarily related to the

mechanical performance of CuCrZr alloy under irradiation, since there are not so many design options available. Therefore, the fundamental improvement of divertor target performance can be best realized by employing an advanced heat sink material. There have been steady R&D efforts for developing high-performance heat sink materials for the divertor target application. These novel materials are mostly copper-matrix composites aiming at achieving higher strength and toughness, but also reduced thermal stresses.

As a review article this paper presents an overview on the current progress in the development of advanced heat sink materials. For the sake of brevity, we'll consider only selected materials of interest for discussion. It is noted that the data collated here are gathered mostly from the previous publications of author's group. Thus, they do not cover the whole hitherto achieved progress reported so far in the literature. The aim of this paper is to provide the readers with a rationale for material design and the state-of-the-art material concepts as a potential reference for their metallurgical development.

2. Performance of CuCrZr alloy under irradiation

At first, we begin with a brief discussion on the design/material interface issue related to the heat sink application of CuCrZr alloy for DEMO divertor target. In the literature, there are a limited number of, yet highly valuable tensile test data of irradiated CuCrZr alloy obtained from irradiation test campaigns carried out at DEMO-relevant temperature range (100-350 °C) and neutron dose (1-10 dpa) [10-13]. The trend of these experimental data can be summarized as follows:

1. CuCrZr alloy exhibits substantial thermal recovery of cascade defects when irradiated above 250 °C. At 250 °C the uniform elongation is recovered up to about 4 % which is sufficiently large for preventing brittle failure.
2. CuCrZr alloy exhibits apparent embrittlement when irradiated below 200 °C where the uniform elongation is decreased down to 1-2 %. With such embrittlement the tensile-stressed part of a heat sink is likely to undergo necking and damage.
3. Notwithstanding the significant reduction in uniform elongation, CuCrZr alloy shows considerable total elongation before rupture up to about 8 % at lower temperatures say, 150 °C.
4. The fracture toughness of CuCrZr alloy is only moderately reduced by irradiation even at low temperatures, e.g. 80 °C.

5. Under long-term thermal exposure CuCrZr alloy exhibits significant loss of strength at elevated temperatures above 400 °C by over-ageing and creep. Softening is further fostered when irradiated at 300-350 °C owing to irradiation creep effect.

The features described above clearly suggest that CuCrZr alloy is subject to upper and lower temperature limits in order to be operated under irradiation without shortfall of any structural functionality as heat sink.

3. Structural requirement for a water-cooled heat sink

The baseline design concept being currently considered for the water-cooled divertor target of a DEMO reactor is the ITER-like tungsten monoblock model equipped with a CuCrZr cooling tube as heat sink [5, 14]. An extensive finite element analysis of the HHF loading behavior of a typical tungsten monoblock target (W armor thickness: 5 mm) delivered following features [15]:

1. At the coolant temperature of 150 °C the CuCrZr heat sink is heated up to ca. 260 °C under heat flux of 10 MW/m² and to ca. 350 °C under 18 MW/m².
2. Under the same condition, the peak temperature at the tube inner wall reaches up to ca. 230 °C and 290 °C, respectively. In this temperature range CuCrZr alloy is likely to suffer from considerable corrosion depending on water chemistry [16].
3. The temperature in the heat sink tube is predominantly below 200 °C even under 18 MW/m².
4. Thermal stress develops upon cooling while being relieved during HHF loading. The thermal stress is concentrated in the upper region of the cooling tube where heat flux is concentrated.
5. If the CuCrZr heat sink maintains the initial strength with prime-aged microstructure, the plastic strain is produced during the fabrication process only. In the course of the cyclic HHF loading the heat sink readily enters into an elastic shakedown regime, thus excluding the risk of low cycle fatigue.
6. On the contrary, the soft copper interlayer undergoes heavy plastic fatigue due to large incremental plastic deformation. This implies a possibility that the CuCrZr heat sink may also experience plastic fatigue, when it should be operated in the irradiation creep regime and thus be softened or damaged.

Fig. 1 illustrates the three kinds of design stress limit data of irradiated CuCrZr alloy for the relevant operation temperature range [12]. Plotted are the elastic stress limits S_d, S_e and S_m,

collated in the ITER SDC-IC code. Each of these design stress limits is related to one of the non-brittle structural failure criteria formulated in the SDC-IC, respectively: immediate local fracture due to exhaustion of ductility, immediate plastic flow localization and progressive plastic deformation (ratchetting). Also indicated are the major design constraints of a water-cooled divertor target in form of a bar code, namely, the desired optimal coolant temperature ($T \leq \sim 150$ °C), the temperature range where severe corrosion is expected (~ 200 °C $\leq T$) and the most probable operation temperature range of a CuCrZr heat sink (~ 150 °C $\leq T \leq \sim 380$ °C) under heat flux fluctuations between 10-18 MW/m².

The data curves in this diagram clearly show a drastic trade-off effect of temperature between ductility (S_e) and strength (S_m) in the range from 200 °C to 350 °C. From the structural design point of view, the best operation temperature range for the irradiated CuCrZr heat sink seems to be between 250 °C and 300 °C, the overlapping band of acceptable S_e and S_m. Of course, this range is obviously too narrow to realize under the foreseen HHF loads. This unfortunate circumstance strongly suggests the need of novel high-performance heat sink materials which could enable one to extend the allowable operation temperature range in both directions. In the following chapters the basic rationale for materials design is explained and three distinct examples of such candidate materials are presented.

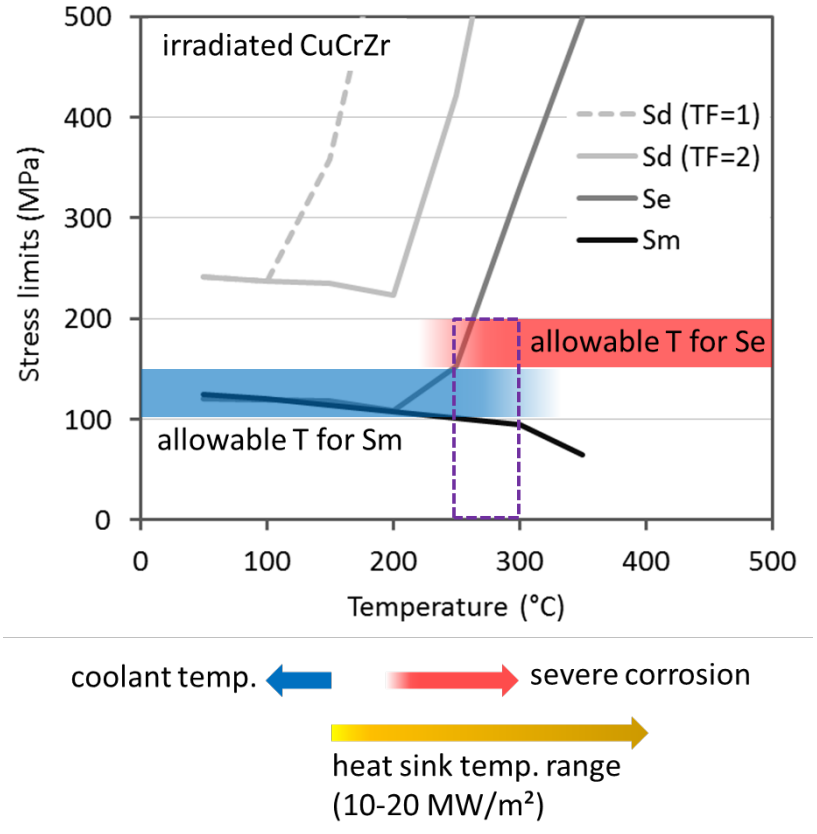

Fig. 1. Selected stress limits of CuCrZr alloy from the SDC-IC code plotted as a function of temperature. The subscript ‘irr’ and ‘unirr’ stands for the data of an irradiated and pristine specimen, respectively [12].

4. Rationale for materials design for heat sink

The rationale for materials design can be directly derived from the gap between the previously addressed design requirements of the heat sink and the actual performance limit of the copper alloys. In the following some key elements of the rational considered here are summarized,

1. Very high thermal conductivity (> 250 W/m·K) with acceptable activation and ductility as paramount prerequisite. In this regard, only copper-base materials come into question.
2. High tensile strength at elevated temperatures (≤ 400 °C). The requirements 1 and 2 can be best reconciled in form of a composite material consisting of copper matrix and high-strength reinforcements. The reinforcements should have a refractory nature.
3. The properties of a heat sink composite should be tailored in such a way that the mismatch of elastic constants and thermal expansion coefficient (CTE) between the armor (i.e. tungsten) and the heat sink is reduced as much as possible.
4. The design and fabrication of the composites should allow flexible adaptation to design for optimization. Fibrous or particulate reinforcements offer such flexibility.
5. The fabrication technology should be compatible with the component manufacture process.
6. The candidate composites should possess plenty of internal interfaces which may act as a barrier to crack propagation or a site of energy dissipation upon debonding, when embrittled.

Taking this rationale into account, three different types of composite materials are considered in this article. In the following chapters the recent progress and the state-of-the-art of the candidate materials are presented.

6. SiC fiber-reinforced Cu composite

6.1. Motivation

Long SiC fibers have been widely used as high-strength or high-modulus reinforcements for various kinds of metal matrix or ceramic matrix composites. For instance, titanium matrix composites reinforced with continuous SiC fibers have been developed for high-temperature lightweight structural applications such as turbine rotor ring of aircraft engines in industrial maturity [17].

Based on the similar concept and fabrication route, but aiming at HHF applications, long SiC fibers were applied to copper matrix to develop PFCs with Cu/SiC_f composite heat sink since early 2000s [18-24]. There are various commercial products of SiC_f fibers with a wide span of properties and diameters (∅: 10-140 μm). For developing Cu/SiC_f composites only thick fibers (∅ > 100 μm) were employed for the sake of easy manual handling in laboratory processing.

To date, two commercial products, Sigma^{TM} fiber (∅: 105 μm) and SCS6^{TM} fiber (∅: 142 μm), have been used for the R&D of Cu/SiC_f composites [22, 23]. The ultimate tensile strength of the SiC_f fibers ranges between 3.2 (Sigma) and 4.4 (SCS6) GPa. The fracture strain is around 0.8 (Sigma) or 1 (SCS6) %. The effective Young's modulus ranges between 340 (Sigma) and 400 (SCS6) GPa. The Weibull modulus of fracture stress is around 15. The major virtues of SiC_f fibers are the excellent high-temperature strength and benign neutron irradiation behavior (low activation, low helium production, low swelling and low mechanical impairment). The CTE of a SiC fiber is around 4.5 microstrains per Kelvin.

On the other hand, the quite low thermal conductivity (~16 W/m·K) of SiC_f fibers may seem to be a concern for heat sink application [25]. However, the measured thermal conductivity data of actually fabricated Cu/SiC_f composites (Sigma) reveal that the thermal conductivity is far from being 'too bad' to be used as heat sink. The conductivity is kept above 170 W/m·K at the fiber volume fraction (V_f) of 29 % and above 200 W/m·K at the V_f of 23 % up to 500 °C as shown in Table 1 [23]. This result is highly encouraging, since the strengthening effect by the fibers begins to be significant already at V_f of about 20 % as will be shown later.

Table 1. Thermal conductivity data of fabricated Cu/SiC_f composites (Sigma fiber) measured by laser flash method [23].

V_f	300 °C	400 °C	500 °C
22%	214	208	213
28%	176	173	173
37%	140	136	131

Fig. 2 shows the typical microstructure of a Cu/SiC_f composite (Sigma) imaged by confocal laser microscopy. The composite in this micrograph had already undergone long-term thermal exposure at 550 °C for 400 hours [24]. The fibers exhibit slight damage in form of a pore or crack which were absent in the as-fabricated state. However, the interfaces and the matrix remained mostly intact after the thermal loading. Here, the fibers were arrayed in an irregular

pattern owing to manual fabrication, but an ordered array should be also possible, provided an instrumented textile machine is employed. The grey scale contrast reveals the constituent materials (W core, C-rich SiC, β-SiC, C coat) in the fibers and grains (twins) in the matrix.

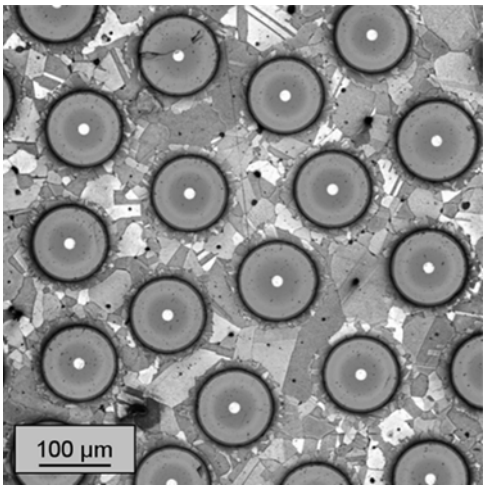

Fig. 2. Confocal laser micrograph image of a Cu/SiC_f composite (Sigma fiber) after thermal exposure at 550 °C for 400 hours [24].

6.2. Properties

The longitudinal ultimate tensile strength of unidirectional Cu/SiC_f composites exhibits a rule-of-mixture behavior, provided the microstructure is intact. In Fig. 3 the tensile strength data of unidirectional Cu/SiC_f composites are plotted for the V_f range from 15 to 40 %. The data were obtained for two different kinds of Cu/SiC_f composites, each reinforced with Sigma or SCS6 fibers and tested at RT and 300 °C, respectively [23].

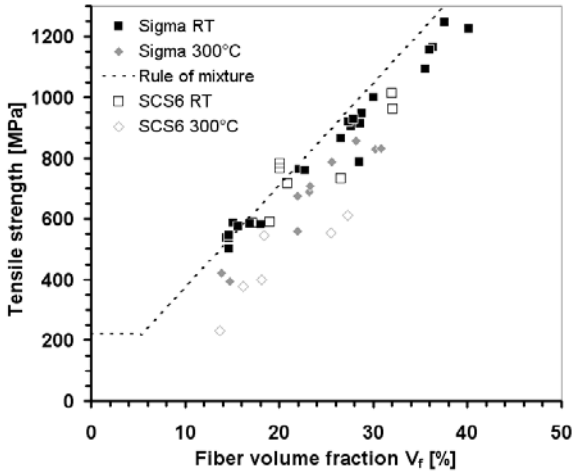

Fig. 3. Ultimate tensile strength data of two kinds of Cu/SiCf composites (solid symbols: reinforced with Sigma fibers, open symbols: SCS6 fibers) [23].

At RT both types of Cu/SiC_f composite reached nearly theoretical strength values as predicted by the rule-of-mixture. When tested at 300 °C, however, the composites exhibit more or less reduced strength. In particular, Cu/SiC_f composite exhibits more significant strength reduction when reinforced with SCS6 fibers than with Sigma fibers. On the contrary, the Cu/SiC_f with Sigma fibers seems to undergo only moderate degradation. This data plot clearly demonstrates the highly effective reinforcing effect of SiC fibers even at 300 °C. The tensile strength of the Cu/SiC_f composite (Sigma) reaches nearly 800 MPa already at the V_f of 30 % at 300 °C. This strength value may surpass by far the typical maximum tensile stress in the divertor heat sink. The Young's modulus of the composites approximately follows the rule-of-mixture as well in the axial direction.

Fig. 4 shows the tensile curves of two unidirectional Cu/SiC_f composites (Sigma fiber) tested at RT, each with V_f of 16 % and 40 %, respectively [23]. As expected, the global fracture strain in the axial direction is determined by the fracture strain of the SiC fiber which lies around 0.8 %. In contrast to the high-V_f composite which fully breaks immediately after the peak stress, the low-V_f composite exhibits considerable residual stress even after the overall fracture of fibers. This is owing to the plastic work and strain hardening of the load-carrying Cu matrix. Such extensive plastic straining is not possible in the high-V_f composite, since the volume of the Cu is too small so that the yield criterion can hardly be met while hydrostatic stress may develop strongly.

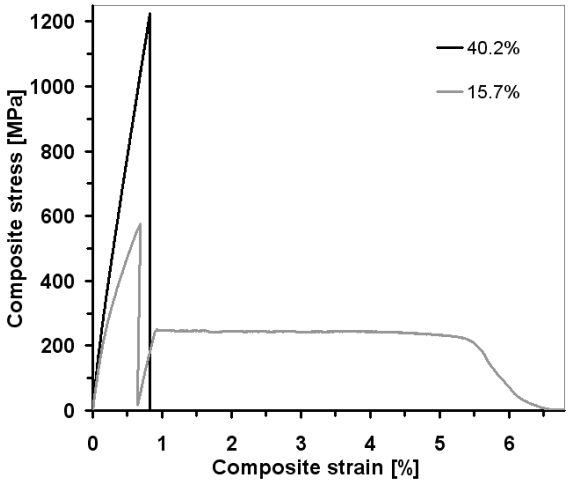

Fig.4. Tensile curves of two unidirectional Cu/SiC_f composite (Sigma fiber) tested at RT. (V_f: 16 % and 40 %). The stress-strain curves were measured in longitudinal direction [23].

Strong and thermally stable bonding of fiber/matrix interface is a critical requirement to reach high strength of Cu/SiC_f composites. To realize such interface titanium thin film (thickness: < 1 µm) is coated on the outer surface of carbon-coated SiC fiber forming a refractory carbide film during HIP (hot isostatic pressing) process. This TiC film is stronger than the internal SiC/C interface as shown in Fig. 5 which shows a protruded fiber after a single fiber push-out test [23]. The outer C mantle was separated from the main body of the SiC fiber while stuck to the Cu matrix.

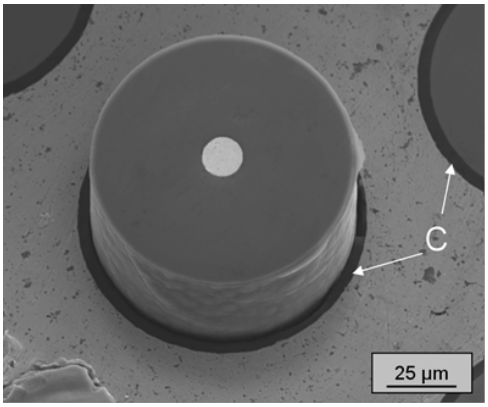

Fig. 5. SEM image of a protruded SiC fiber (Sigma) in a Cu/SiC_f composite after a fiber push-out test [23].

The soundness and integrity of SiC fibers in Cu/SiC_f composites is important for maintaining the thermal stability of microstructure and strength at high temperatures. This issue may be particularly critical in the case of Sigma fiber, as it contains a substantial amount of residual silicon solutes. During long-term thermal exposure failure of C mantle and cracking of a SiC fiber may cause massive diffusion of Cu into SiC forming brittle intermetallic phases leading to a significant reduction of strength. Fig. 6 illustrates a failed SiC fiber (Sigma) in a Cu/SiC_f composite after thermal exposure at 550 °C for 400 hours. The bright gray region indicates brittle intermetallic phases (cupper silicides) [24].

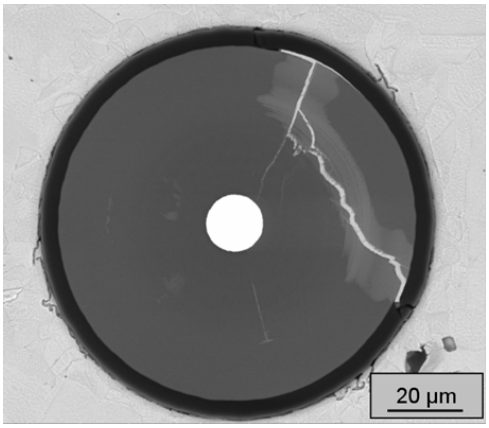

Fig. 6. SEM image of a failed SiC fiber (Sigma) in a Cu/SiC_f composite after thermal exposure at 550 °C for 400 hours [24].

6.3. Eligible design concept

Due to the high stiffness and brittleness thick SiC fibers allow only such fiber architectures that have either a straight array or a gentle curvature. This limitation has the consequence that the most feasible geometry of a Cu/SiC_f composite heat sink should be of a rectangular form. In this sense, a Cu/SiC_f composite might be best utilized for strengthening the Cu alloy heat sink of a flat-tile type divertor target as illustrated in Fig. 7. In the flat-tile type target model thermal stresses are dominated by the mismatch in CTEs between W and Cu. Thus stresses are locally concentrated near the bond interface. As only the highly stressed region needs to be reinforced, several stack layers (ca. 10) would be sufficient for strengthening [19, 20].

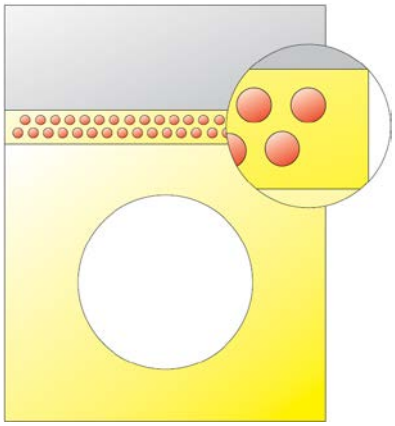

Fig. 7. Schematic illustration of a feasible configuration of a flat-tile type divertor target with a Cu/SiC_f composite laminate as reinforcing interlayer [19].

The intensity of interfacial stress concentration can be substantially reduced by the presence of a composite interlayer owing to reduced mismatch in thermal strain, as the elastic constants and the CTE of a Cu/SiC_f composite would be of intermediate values between those of W and

Cu [18, 26]. As a consequence, the driving force of interfacial cracking is reduced accordingly as shown in Fig. 8. Fig. 8 plots the variation of J-integral values at an interfacial crack tip (crack length: 0.5 mm) of a flat-tile type target (cf. Fig. 7) during a HHF load cycle (heat flux: 15 MW/m², pulse duration: 30 s). Upon HHF loading the interfacial stress intensity rapidly decreases from the maximum in the residual stress state and increases again upon cooling. It is seen that the cyclic amplitude of J-integral is much smaller in the presence of Cu/SiCf composite interlayer than the conventional target [19]. This effect is indeed beneficial for the integrity of the bond interface, as it is the most vulnerable site in a flat-tile type target.

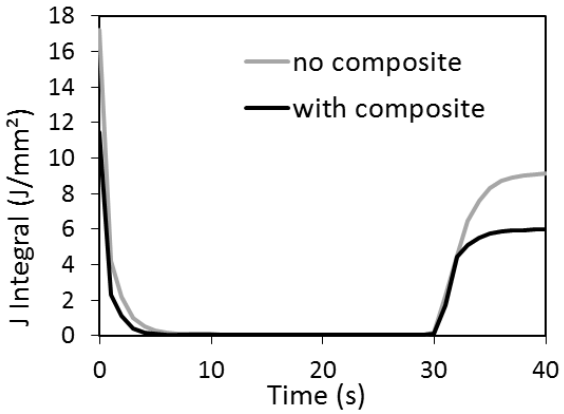

Fig. 8. Variation of J-integral values at an interfacial crack tip (crack length: 0.5 mm) of a flat-tile type target during a HHF load cycle (heat flux: 15 MW/m², pulse duration: 30 s) [19].

A dedicated micromechanics study showed that the embedded SiC fibers would experience only compressive stress during the whole HHF load cycle of a flat-tile target as shown in Fig. 9 [19]. Fig. 9 plots the variation of the maximum principal stress in the fiber and the matrix of the Cu/SiCf composite interlayer (cf. Fig. 7) during a HHF load cycle (heat flux: 15 MW/m², pulse duration: 30 s). Although the magnitude of fiber stress is fairly high, the compressive stress would not cause any fracture of the fiber. This is also a beneficial feature in view of the mechanical reliability of fiber.

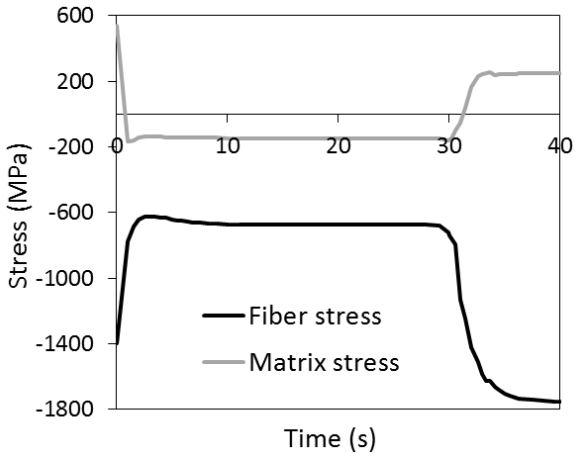

Fig. 9. Variation of the maximum principal stress in the fiber and the matrix of the Cu/SiC_f composite interlayer of a flat-tile type target during a HHF load cycle (heat flux: 15 MW/m², pulse duration: 30 s) [19].

6.4. HHF performance

The overall HHF performance of a Cu/SiC_f composite heat sink was evaluated by means of HHF fatigue tests using a dedicated test mock-up as shown in Fig. 10 (a) [27]. The mock-up consisted of 8 tungsten flat-tiles as armor, a Cu/SiC_f composite interlayer and a water-cooled CuCrZr heat sink block. The three parts were joined by means of brazing. The cross section of the composite interlayer is shown in Fig. 10 (b). The Cu/SiC_f interlayer had a thickness of 2.5 mm and consisted of 4 unidirectional stacks of fiber lamina (V_f : 14 %).

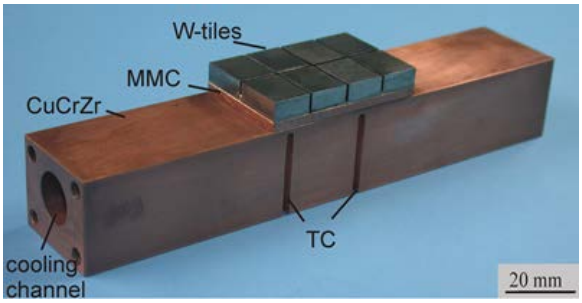

Fig. 10 (a). HHF test mock-up consisting of 8 tungsten armor tiles, a Cu/SiC_f composite interlayer and a water-cooled CuCrZr heat sink block [27].

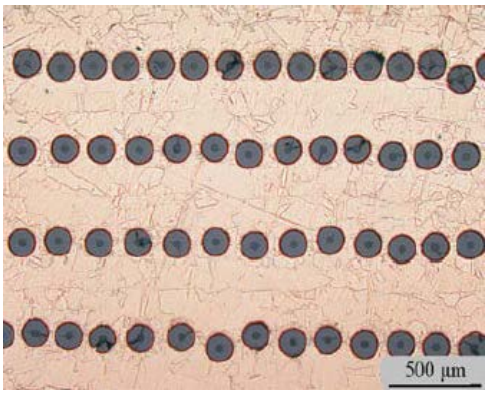

Fig. 10 (b). Metallographic cross section of the unidirectional Cu/SiC_f composite interlayer in the test mock-up after HHF test at 10.5 MW/m² after 80 load cycles [27].

It was demonstrated that the mock-up withstood HHF loads of at least 10 MW/m² under hydrogen beam irradiation with water cooling at RT. Fig. 11 illustrates the in-situ images of infrared red thermography (a) and photography (b), respectively, measured during a HHF fatigue test at 10.5 MW/m² after 40 loading cycles [27]. The color contrast reveals that one tile failed while the other tiles remained still intact. Among the 8 tested armor tiles 7 tiles survived at least 80 load cycles. The premature failure was found to be interface debonding due to a fabrication flaw.

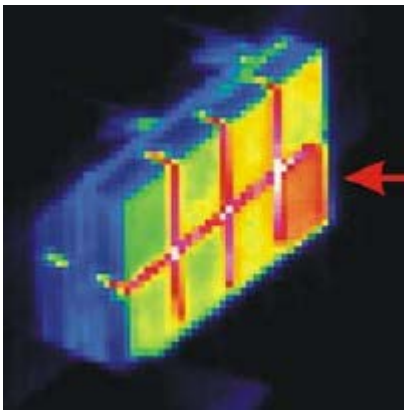
(a)
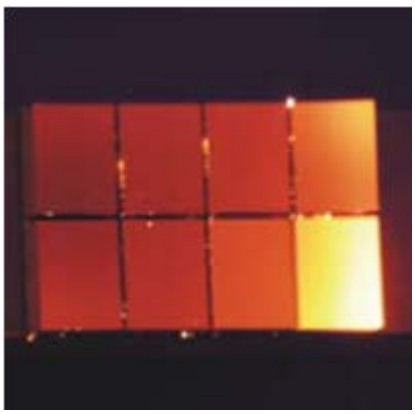
(b)

Fig. 11. In-situ images of infrared red thermography (a) and photography (b) measured during HHF fatigue test at 10.5 MW/m² after 40 loading cycles [27].

The metallographic image of the Cu/SiC_f interlayer in Fig. 10 (b) shows the post-mortem microstructure of the composite after the HHF test stated above. Conspicuous failure is found in several SiC fibers, though the majority of the fibers and the matrix remained mostly intact. A finite element analysis estimated that the Cu/SiC_f interlayer is stressed up to 400 MPa (von Mises) and the temperature profile ranges from 400 to 600 °C (W armor: 1040 °C) for the

given HHF test condition. The predicted maximum stress level seems to be allowable for the fiber axial orientation, but may be too high for the transverse orientation, since the transversal strength is much lower than the axial strength. Thus, a cross ply laminate architecture would be more advantageous in view of strengthening strategy. The maximum temperature (600 °C) experienced by the Cu/SiC_f interlayer seems rather too high to preserve the chemical stability of the fiber/matrix interface for long-term operation. Hence, thermal management would be a challenging issue for this Cu/SiC_f interlayer concept.

7. W wire-reinforced Cu composite

7.1. Motivation

Tungsten wires are characterized by excellent tensile strength, remarkable flexural flexibility and notable ductility. Fig. 12 plots the typical tensile curves of a commercial tungsten wire (diameter: 125 μm) before and after heat treatment at 1000 °C for 10 hours. The ultimate tensile strength reached 2.3-2.5 GPa and the rupture strain was no less than 2.3 %, which is relatively high compared to other kinds of high-strength fibers. High-temperature annealing is found to improve ductility while strength is slightly reduced.

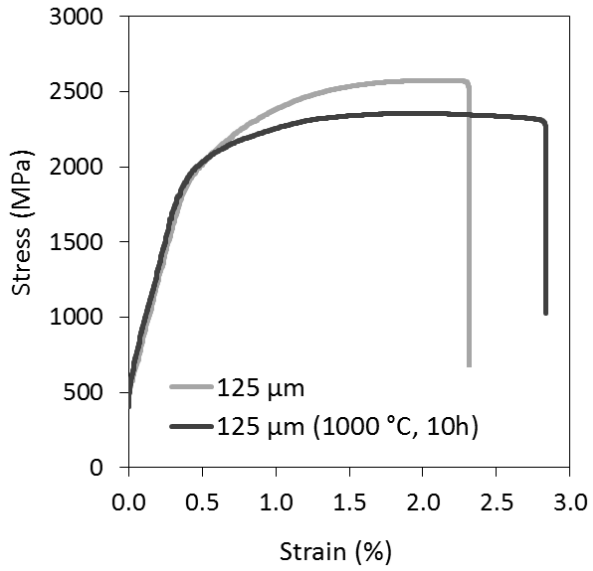

Fig. 12. Typical tensile curves of a commercial tungsten wire (diameter: 125 μm) before and after heat treatment at 1000 °C for 10 hours.

Fig. 13 shows the fractographic images of the rupture surface of a commercial tungsten wire (diameter: 125 µm) after a tensile test. In Fig. 13 (a) the wire exhibits apparent plastic necking in the vicinity of rupture site indicating that substantial plastic deformation took place locally. The microscopic image of the fracture surface in Fig. 13 (b) reveals that the overall fracture was initiated by local plastic rupture of individual long grains aligned longitudinally. This microscopic rupture feature explains the origin of the global ductility of tungsten wires.

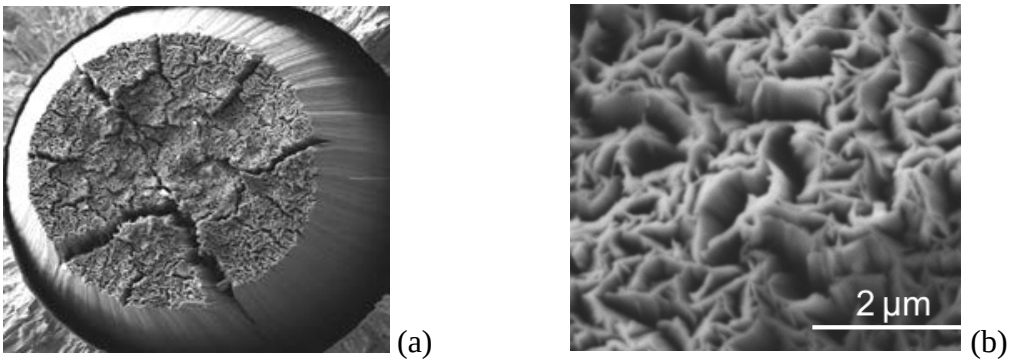

(a) (b)

Fig. 13. Fractographic images of the rupture surface of a commercial tungsten wire (diameter: 125 µm) after a tensile test. (a): whole ruptured cross section, (b): microscopic image of the fracture surface.

The ductility of tungsten wires, although being moderate, has a huge effect on the statistical reliability of tungsten wires against failure. In Fig. 14 four Weibull plots of tensile strength are presented for two different kinds of tungsten wires (diameter: 75 and 125 µm), each with and without heat treatment at 1000 °C for 10 hours. The Weibull parameters extracted from these plots range from 190 to 220 which is very high. The large Weibull parameters indicate that the statistical scattering of strength data of tungsten wires is extremely small.

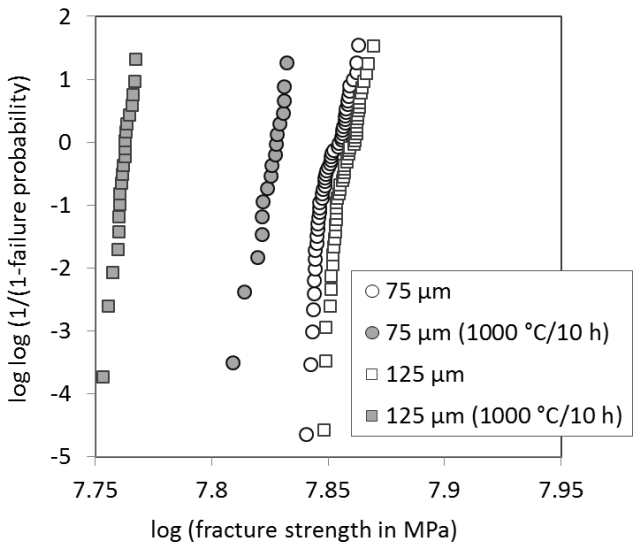

Fig. 14. Weibull plots of tensile strength plotted for two different kinds of tungsten wires (diameter: 75 and 125 µm), each with and without heat treatment at 1000 °C for 10 hours.

The combination of very high strength and moderate ductility is an ideal condition for use as fibrous reinforcement. The resulting toughness and flexural flexibility enables easy handling and high-curvature winding in manufacture process. Tungsten wires offer further advantages such as high thermal conductivity, excellent wettability and insolubility in copper, refractory nature and diverse commercial availability. All these beneficial properties make tungsten wire uniquely attractive as reinforcement material.

Fig. 15 shows a micrograph of the metallographic section of a tungsten wire-reinforced copper composite (W_f/Cu) fabricated by HIP process [28]. Dense wire packing without matrix pore or interfacial defect is demonstrated.

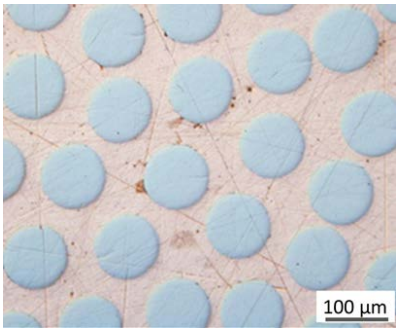

Fig. 15. Micrograph of the metallographic section of a W_f/Cu composite.

7.2. Properties

W_f/Cu composites have been extensively characterized already in 1950's by the researchers at NASA as an ideal model system for investigating fiber-reinforced metal matrix composites [29, 30]. Comprehensive reviews on the properties of W_f/Cu composites are found elsewhere [31]. According to the NASA reports, the most remarkable feature of the mechanical behaviors of W_f/Cu composite materials is the fact that the major strength properties such as ultimate tensile stress, yield stress and stress-rupture stress as well as physical properties such as elastic modulus and thermal conductivity obey the rule-of-mixtures nearly perfectly over a wide range of wire volume fraction. This outstanding quality feature is owing to the toughness of tungsten wires and excellent interfacial adhesion. In Table 2 selected material properties of W_f/Cu composites are summarized [31]. The data shows that one can achieve a pronounced strengthening effect without sacrificing the thermal conductivity too much by means of tungsten wire reinforcement.

Table 2. Selected material properties of W wire-reinforced Cu composites [31].

	V_f: 20 %	V_f: 40 %
ultimate tensile stress (MPa)	500 (RT) 330 (650 °C) 290 (810 °C)	960 (RT) 540 (650 °C) 500 (810 °C)
yield stress (MPa)	470 (RT)	920 (RT)
stress-rupture stress (MPa) at 1000 hours	220 (650 °C) 180 (810 °C)	420 (650 °C) 320 (810 °C)
thermal conductivity (W/m·K)	300 (RT)	235 (RT)

7.3. Eligible design concept

The high flexural flexibility of tungsten wires allows fabrication of a cylindrical composite tube with a relatively small diameter (10-12 mm) and thickness (1-2 mm). Using a thin wire (diameter: ca. 100 µm), production of a W_f/Cu composite tube with a multilayered winding architecture is also feasible. This technical possibility fits very well with the geometry of a monoblock-type divertor target. Fig. 16 illustrates one of the candidate design concepts which incorporate an integrated W_f/Cu composite tube as heat sink [32]. The zoom lens highlights the multiply wound architecture of wire-reinforcement in a schematic way.

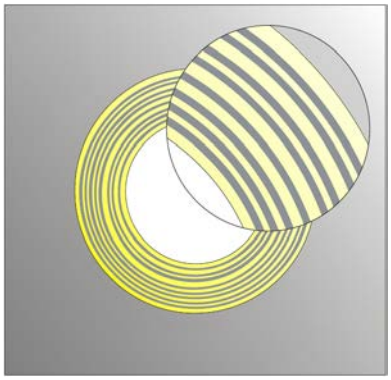

Fig. 16. Schematic illustration of a feasible design concept of a W monoblock-type divertor target with a W_f/Cu composite tube [32].

A rigorous finite element simulation study of HHF loading behavior was carried out by the author by use of a dedicated micromechanics-based elasto-plastic constitutive equation [32]. The dual scale stress analysis delivered a positive prediction that the maximum tensile stress of the reinforcing tungsten wires in the W_f/Cu composite tube would not exceed the ultimate tensile strength of the W wire. The result of this stress assessment is given in Fig. 17 where

the profile of tungsten wire stress is plotted along the thickness direction of the W_f/Cu tube at the most stressed region (nearest to the heat-loaded surface) in a W monoblock-type divertor target. The graph shows that the highest stress would occur at the tube inner wall in the residual stress state after fabrication while the thermal stress would be significantly relieved upon HHF loading. The local peak stress under a typical HHF load reaches roughly 1600 MPa, which is indeed far below the tensile strength of W wire.

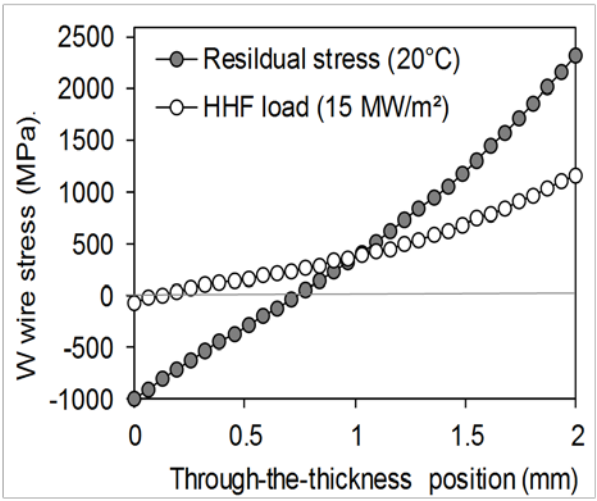

Fig. 17. Profile of tungsten wire stress plotted along the thickness direction of the W_f/Cu composite cooling tube at the most stressed region in a W monoblock-type divertor target. Stress profiles are plotted for two different stages of a HHF load cycle [32].

7.4. HHF performance

A HHF loading test was conducted by the researchers at the IPP Garching on a water-cooled tungsten monoblock mock-up equipped with a W_f/Cu composite cooling tube. The test mock-up is shown in Fig. 18 [33]. The W_f/Cu composite tube was fabricated using cross winding of wires by means of hot isostatic pressing at 650 °C and 100 MPa for a half hour. The tube was then joined to four tungsten blocks by brazing. Under a HHF loading test at 10 MW/m² two blocks were cracked at the braze interface in the early stage of test due to fabrication defect while the other two blocks withstood 25 load cycles without failure. The temperature of the inner tube reached up to 250 °C at the coolant temperature of 15 °C.

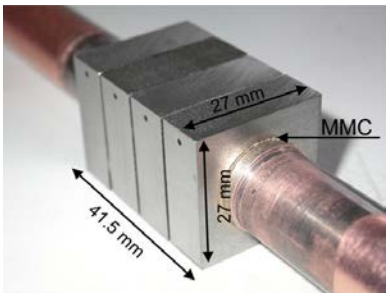

Fig. 18. Water-cooled tungsten monoblock test mock-up with a W_f/Cu composite cooling tube [33].

Fig. 19 shows the metallographic cross section of a successfully tested block of the mock-up after 25 thermal load cycles at 10 MW/m². It is found that both the brazed interface and the wire/matrix interfaces in the composite remained fully intact indicating obviously promising performance.

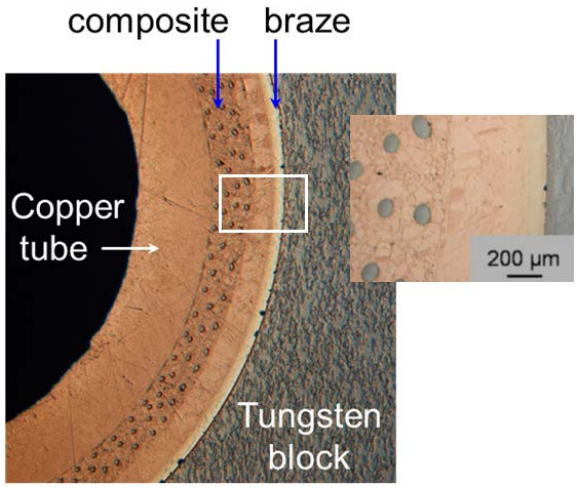

Fig. 19. Metallographic cross section of a successfully tested block of the mock-up after 25 thermal load cycles at 10 MW/m² [33].

8. W particle-reinforced Cu composites

8.1. Motivation

One of the conventional forms of W/Cu composites is the mixture of tungsten particulates as reinforcing constituent and copper matrix. Such W particle-reinforced Cu composites (W_p/Cu) offer similar merits as W_f/Cu composites do. Power-metallurgical routes are well-established to fabricate W_p/Cu composites. Recently, the researchers at IFAM Dresden developed a two-step fabrication process [34]. In the first step, a porous skeleton made of tungsten particles is produced by means of power-metallurgical techniques (compaction, debinding and sintering)

with tailored porosity. In the second step, copper alloy melt is infiltrated into the pores with the help of pressure. This technique is quite straightforward, allows near-net-shape production with a graded composition and can be scaled up for industrial manufacture.

In the same way as W_f/Cu composites do, W_p/Cu composites offer dual benefits, namely, (local) strengthening of heat sink and reduction of thermal stress through reduced thermal strain mismatch. The metallurgical flexibility in terms of processing and microstructural design makes W_p/Cu composites highly attractive for the engineering of water-cooled divertor target.

Fig. 20 is a scanning electron micrograph showing the microstructure of a W_p/Cu composite with the V_f ratio of 50:50 (the bright phase stands for tungsten). It is found that the tungsten skeleton is completely filled with copper owing to the excellent wettability between tungsten and copper.

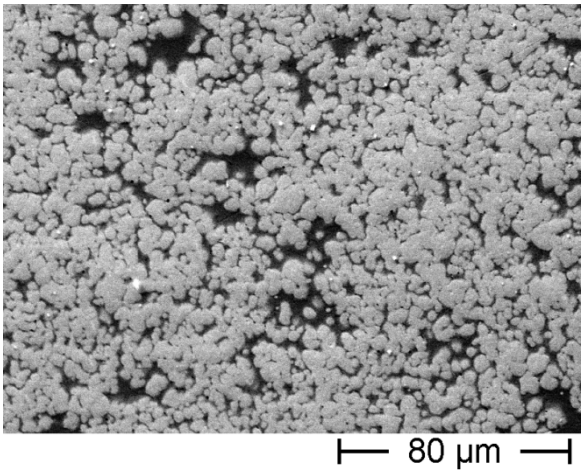

Fig. 20. Microstructure of a W_p/Cu composite with the V_f ratio of 50:50 (the bright phase stands for tungsten) [34].

8.2. Properties

Selected material properties of W_p/Cu composites are summarized in Table 3 [34]. The two reference materials (V_f: 30 %, 50 %) used for the measurement were fabricated by the IFAM processing route. Typical tensile stress-strain curves of W_p/Cu composites (tungsten V_f: 50 %) obtained at three test temperatures are plotted in Fig. 21.

The ultimate tensile stress data indicates a significant strengthening effect of the composites in comparison to monolithic CuCrZr alloy, in particular, at the higher V_f of tungsten. In the

case of V_f = 50 %, the tensile strength is increased by more than 40 % at 300 °C and nearly 50 % at 550 °C.

On the other hand, ductility is strongly reduced by tungsten inclusions compared to the high ductility of CuCrZr. The failure strain data exhibit a notable scattering. In spite of the strong reduction of total elongation, the ultimate tensile strain values are still larger than the expected strain range (~ 1 %) in the heat sink, thus posing no critical structural issue.

The thermo-elastic properties of W_p/Cu composites lie within the intermediate range between those of tungsten and copper. Thus, the potential of the tungsten reinforcement to mitigate the thermal strain mismatch between armor and heat sink is obviously implied.

Table 3. Selected material properties of W particle-reinforced Cu composites [34].

	V_f of W: 30 %	V_f of W: 50 %
ultimate tensile stress (MPa)*	353 (300 °C) 184 (550 °C)	450 (300 °C) 253 (550 °C)
total elongation (%)	10-12 (300 °C) 4-7 (550 °C)	5-6 (300 °C) 3-6 (550 °C)
Young's modulus (GPa)	155 (300 °C) 130 (550 °C)	175 (300 °C) 160 (550 °C)
coefficient of thermal expansion ($\times 10^{-6}$)	13.3 (150 °C) 14.4 (550 °C)	9.7 (150 °C) 10.3 (550 °C)
thermal conductivity (W/m·K)	300 (300 °C) 307 (600 °C)	240 (300 °C) 244 (600 °C)

*CuCrZr alloy: 318 MPa at 300 °C, 170 MPa at 550 °C.

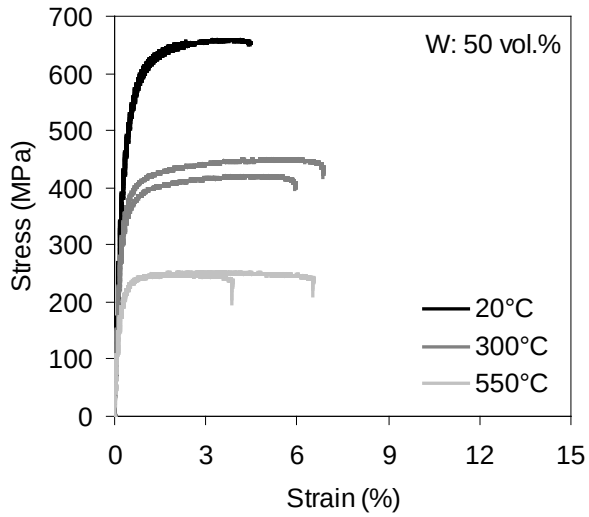

Fig. 21. Typical tensile stress-strain curves of W_p/Cu composites (tungsten V_f: 50 %) obtained at three test temperatures [34].

8.3. Eligible design concept

Owing to the relatively high thermal conductivity, high-temperature strength and acceptable toughness as structural material, W_p/Cu composites is best suitable for bulk heat sink rather than a tube. As direct exposition of copper to plasma has to be avoided, covering of tungsten armor with sufficient thickness is still needed. The resulting design solution is the flat tile type target concept consisting of tungsten flat tile armor, W_p/Cu composite heat sink block and CuCrZr cooling tube bonded to the composite via copper interlayer as illustrated in Fig. 22. W_f/Cu composite could replace the copper alloy as well for the cooling tube.

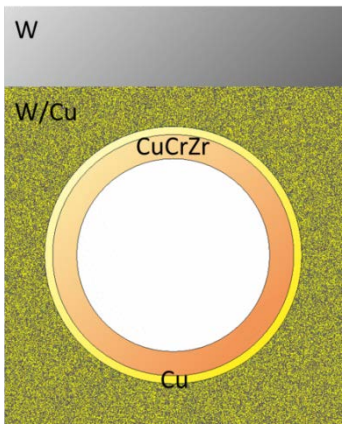

Fig. 22. Flat tile type composite target concept consisting of tungsten flat tile armor, W_p/Cu composite heat sink block and CuCrZr alloy (or W_f/Cu composite) cooling tube bonded to the composite via Cu interlayer.

8.4. HHF performance

In order to evaluate the structural reliability of W_p/Cu composite material under cyclic HHF loads, a simplified demonstrator mock-up was fabricated as illustrated in Fig. 23 [35]. The test mock-up consisted of castellated tungsten tiles, CuCrZr alloy heat sink block with a cooling channel and functionally graded W_p/Cu composite interlayer between the armor and heat sink. The composite interlayer again consisted of three layers each with a different composition (V_f: 30, 50, 70 %), respectively. The layers had thickness of about 1.5 mm each.

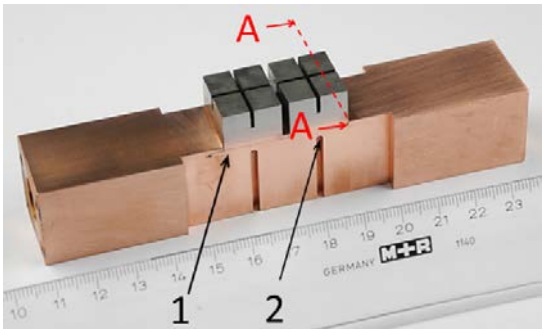

Fig. 23. Test mock-up consisting of castellated tungsten tiles, CuCrZr alloy heat sink block with a cooling channel and functionally graded W_p/Cu composite interlayer between the armor and heat sink. The composite interlayer consisted of three layers (thickness: 1.5 mm for each) each with a different composition (V_f: 30, 50, 70 %), respectively [35].

Cyclic HHF tests were conducted on three mock-ups at a hydrogen beam irradiation facility (GLADIS). All mock-ups withstood HHF loads of 15 MW/m² up to 50 load cycles without failure (coolant temperature: RT). One of the mock-ups could survive even 20 MW/m². Fig. 24 shows a micrograph of the metallographic section of the W_p/Cu composite interlayer after a HHF test at 20 MW/m² (3 cycles) demonstrating an intact microstructure with no defect [35].

Fig. 24 shows a micrograph of the metallographic section of the W_p/Cu composite interlayer after a HHF test at 20 MW/m² (3 cycles) [35].

9. Concluding remarks and outlook

In this article, three most promising Cu-matrix composite materials were reviewed in terms of thermal, mechanical and HHF performance as structural heat sink materials. The considered candidates were W particle-reinforced, W wire-reinforced and SiC fiber-reinforced Cu matrix composites. These composites underwent extensive metallurgical development since a decade and reached a mature engineering stage on a laboratory scale. All of the three composites exhibited far superior ultimate tensile strength at elevated temperatures compared to CuCrZr alloy. In particular, thermal conductivity was not notably affected by the reinforcements up to 50 %. The essential benefits of Cu matrix composites for the heat sink application are two-fold, namely, enhancement of higher-temperature strength and reduction of thermal stress by mitigating the thermal strain mismatch. Cyclic HHF tests demonstrated positive potential that the composite target mock-ups survived several tens of HHF load cycles at 10 or 15 MW/m² without structural or material failure of the composite heat sinks.

For future application to the DEMO divertor target, the industrial scale production technology needs to be developed. In addition, theoretical methodology for the modelling of deformation, damage and fracture needs to be established for the formulation of structural failure criteria. Comprehensive materials test data including irradiation tests are urgently required to support nonconventional structural design efforts.

Acknowledgment

This work has been carried out within the framework of the EUROfusion Consortium and has received funding from the European Union's Horizon 2020 research and innovation programme under grant agreement number 633053. The views and opinions expressed herein do not necessarily reflect those of the European Commission.

References

[1] E. Visca, E. Cacciotti, A. Komarov, et al., Manufacturing, testing and post-test examination of ITER divertor vertical targetWsmall scale mock-ups, Fusion Eng. Des. 86 (2011) 1591-1594.

[2] J. Boscary, B. Böswirth, H. Greuner, et al., Fabrication and testing of W7-X pre-series target elements, Phys. Scr. T128 (2007) 195-199.

[3] M. Matsukawa, M. Kikuchi, T. Fujii, Status of JT-60SA tokamak under the EU-JA Broader Approach Agreement, Fusion Eng. Des. 83 (2008) 795-803.

[4] J. Bucalossi, M. Missirlian, P. Moreau, The WEST project: Testing ITER divertor high heat flux componenttechnology in a steady state tokamak environment, 89 (2014) Fusion Eng. Des. 907-912.
[5] J.H. You, A review on two previous divertor target concepts for DEMO: Mutual impact between structural design requirements and materials performance, Nucl. Fusion, submitted.
[6] R.P. Wenninger, M. Bernert, T. Eich, DEMO divertor limitations during and in between ELMs, Nucl. Fusion 54 (2014) 114003 (8pp).
[7] M.R. Gilbert, S.L. Dudarev, S. Zheng, et al., An integrated model for materials in a fusion power plant: transmutation, gas production, and helium embrittlement under neutron irradiation, Nucl. Fusion 52 (2012) 083019 (12pp).
[8] P. Frosi, S. Villari, G. Ramogida, V. Cocilovo, G. Mazzone, Final Report on Deliverable DIV-1.3.2-01, Load Specification for Divertor Cassette and steel supporting structure for VT and Dome, EFDA_D_2MF3V8, 2014.
[9] V.R. Barabash, G.M. Kalinin, S.A. Fabritsiev, S.J. Zinkle, Specification of CuCrZr alloy properties after various thermo-mechanical treatments and design allowables including neutron irradiation effects, J. Nucl. Mater. 417 (2011) 904-907.
[10] S.A. Fabritsiev, A.S. Pokrovsky, S.J. Zinkle , D.J. Edwards, et al., Low-temperature radiation embrittlement of copper alloys, J. Nucl. Mater. 233-237 (1996) 127-137.
[11] P. Fenici, D.J. Boerman, G.P. Tartaglia, J.D. Elen, et al., Effect of fast-neutron irradiation on tensile properties of precipitation-hardened Cu-Cr-Zr alloy, J. Nucl. Mater. 212-215 (1994) 399-403.
[12] ITER team, ITER structural design criteria for in-vessel components, Appendix A Materials design limit data, G 74 MA 8 01-05-28 W0.2.
[13] M. Li, M.A. Sokolov, S.J. Zinkle, Tensile and fracture toughness properties of neutron-irradiated CuCrZr, J. Nucl. Mater. 393 (2009) 36-46.
[14] F. Crescenzi, C. Bachmann, M. Richou, S. Roccella, E. Visca, J.-H. You, Design optimization of the DEMO ITER-like water-cooled divertor, Fusion Eng. Des. (2015) http://dx.doi.org/10.1016/j.fusengdes.2015.02.056.
[15] M. Li, E. Werner, J.H. You, Low cycle fatigue behavior of ITER-like divertor target under DEMO-relevant operation conditions, Fusion Eng. Des. 90 (2015) 88-96.
[16] S. Wikman, et al. EFDA Report Experimental assessment of erosion corrosion parameters of CuCrZr and CuCrZr/316L(N)-IG joints at simulated plasma and nominal operational ITER conditions, EFDA, 2012.

[17] S.A. Singerman, J.J. Jackson, Titanium metal matrix composites for aerospace applications, Superalloys 1996 (Eds. R.D. Kissinger, et al.), The Minerals, Metals & Materials Society, 1996, 579-586.
[18] J.H. You, H. Bolt, Overall mechanical properties of fiber reinforced metal matrix composites for fusion applications, Journal of Nuclear Materials 305 (2002) 14-20.
[19] J.H. You, Design feasibility study of a divertor component reinforced with fibrous metal matrix composite laminate" J. Nucl. Mater. 336 (2005) 97-109.
[20] J.H. You, Plastic failure risk of a metal-matrix-composite structure under variable thermal loads, Int. J. Mech. Sci. 51 (2009) 816-824.
[21] J.H. You, W. Lutz, H. Gerger, et al. Fiber push-out study of a copper matrix composite with an engineered interface: Experiments and cohesive element simulation, Int. J. Solids Struc. 46 (2009) 4277-4286.
[22] A. Brendel, V. Paffenholz, Th. Köck, H. Bolt, Mechanical properties of SiC long fibre reinforced copper, J. Nucl. Mater. 386–388 (2009) 837–840.
[23] S. Kimmig, I. Allen, J.H. You, Strength and conductivity of unidirectional copper composites reinforced by continuous SiC fibers, J. Nucl. Mater. 440 (2013) 272-277.
[24] S. Kimmig, S. Elgeti, J.H. You, Impact of thermal exposure on a SiC fiber-reinforced copper composite, J. Nucl. Mater. 443 (2013) 386-392.
[25] M. Oksanen, R. Scholz, L. Fabbri, Simple thermal wave method for the determination of longitudinal thermal diffusivity of SiC-based fiber, Review of progress in quantitative nondestructive evaluation. Vol. 17 (Eds. D.O. Thompson, D.E. Chimenti) Plenum Press, New York, 1998.
[26] J.H. You, H. Bolt, Analysis of singular interface stresses in dissimilar material joints for plasma facing components, J. Nucl. Mater. 299 (2001) 1-8.
[27] V. Paffenholz, Synthese und Charakterisierung von SiCf/Cu-Matrix-Verbundwerkstoffen und ihre Anwendung in einem Modell einer Divertor-Komponente, IPP Report, 17/22, 2010.
[28] A. Herrmann, K. Schmid, M. Balden, H. Bolt, Interfacial optimization of tungsten fibre-reinforced copper for high-temperature heat sink material for fusion application, J. Nucl. Mater. 386–388 (2009) 453–456
[29] D.L. McDanels, R.W. Jech, J.W. Weeton, Stress-strain behavior of tungsten fiber reinforced copper composites, NASA TN D-1881, 1963.
[30] D.L. McDanels, R.W. Jech, J.W. Weeton, Analysis of stress-strain behavior of tungsten fiber reinforced copper composites, Trans. Met. Soc. AIME 233 (1965), 636-642.

[31] D.L. McDanels, Tungsten fiber reinforced copper matrix composites, NASA Technical paper 2924, NASA, 1989.
[32] J. H. You, Triple scale failure estimation for a composite-reinforced structure based on integrated modeling approaches: Part l: Micro-scale analysis, Eng. Fract. Mech. 76 (2009) 1425-1436.
[33] A. Herrmann, H. Greuner, M. Balden, H. Bolt, Design and evaluation of an optimized W/Cu interlayer for W monoblock components, Fusion Eng. Des. 86 (2011) 27-32.
[34] J.H. You, S. Nawka, A. Brendel, et al., Thermal and mechanical properties of infiltrated W/CuCrZr composite materials for functionally graded heat sink application, J. Nucl. Mater. 438 (2013) 1-6
[35] H. Greuner, A. Zivelonghi, B. Böswirth, J.H. You, Results of high heat flux testing of W/CuCrZr multilayer composites with percolating microstructure for plasma-facing components, Fusion Eng. Des. (2015) http://dx.doi.org/10.1016/j.fusengdes.2015.02.011.

Figure captions

Fig. 1. Selected stress limits of CuCrZr alloy from the SDC-IC code plotted as a function of temperature. The subscript 'irr' and 'unirr' stands for the data of an irradiated and pristine specimen, respectively [12].

Fig. 2. Confocal laser micrograph image of a Cu/SiC_f composite (Sigma fiber) after thermal exposure at 550 °C for 400 hours [24].

Fig. 3. Ultimate tensile strength data of two kinds of Cu/SiCf composites (solid symbols: reinforced with Sigma fibers, open symbols: SCS6 fibers) [23].

Fig.4. Tensile curves of two unidirectional Cu/SiC_f composite (Sigma fiber) tested at RT. (V_f: 16 % and 40 %). The stress-strain curves were measured in longitudinal direction [23].

Fig. 5. SEM image of a protruded SiC fiber (Sigma) in a Cu/SiC_f composite after a fiber push-out test [23].

Fig. 6. SEM image of a failed SiC fiber (Sigma) in a Cu/SiC_f composite after thermal exposure at 550 °C for 400 hours [24].

Fig. 7. Schematic illustration of a feasible configuration of a flat-tile type divertor target with a Cu/SiC_f composite laminate as reinforcing interlayer [19].

Fig. 8. Variation of J-integral values at an interfacial crack tip (crack length: 0.5 mm) of a flat-tile type target during a HHF load cycle (heat flux: 15 MW/m², pulse duration: 30 s) [19].

Fig. 9. Variation of the maximum principal stress in the fiber and the matrix of the Cu/SiC_f composite interlayer of a flat-tile type target during a HHF load cycle (heat flux: 15 MW/m², pulse duration: 30 s) [19].

Fig. 10 (a). HHF test mock-up consisting of 8 tungsten armor tiles, a Cu/SiC_f composite interlayer and a water-cooled CuCrZr heat sink block [27].

Fig. 10 (b). Metallographic cross section of the unidirectional Cu/SiC_f composite interlayer in the test mock-up after HHF test at 10.5 MW/m² after 80 load cycles [27].

Fig. 11. In-situ images of infrared red thermography (a) and photography (b) measured during HHF fatigue test at 10.5 MW/m² after 40 loading cycles [27].

Fig. 12. Typical tensile curves of a commercial tungsten wire (diameter: 125 µm) before and after heat treatment at 1000 °C for 10 hours.

Fig. 13. Fractographic images of the rupture surface of a commercial tungsten wire (diameter: 125 µm) after a tensile test. (a): whole ruptured cross section, (b): microscopic image of the fracture surface.

Fig. 14. Weibull plots of tensile strength plotted for two different kinds of tungsten wires (diameter: 75 and 125 µm), each with and without heat treatment at 1000 °C for 10 hours.

Fig. 15. Micrograph of the metallographic section of a W_f/Cu composite.

Fig. 16. Schematic illustration of a feasible design concept of a W monoblock-type divertor target with a W_f/Cu composite tube [32].

Fig. 17. Profile of tungsten wire stress plotted along the thickness direction of the W_f/Cu composite cooling tube at the most stressed region in a W monoblock-type divertor target. Stress profiles are plotted for two different stages of a HHF load cycle [32].

Fig. 18. Water-cooled tungsten monoblock test mock-up with a W_f/Cu composite cooling tube [33].

Fig. 19. Metallographic cross section of a successfully tested block of the mock-up after 25 thermal load cycles at 10 MW/m² [33].

Fig. 20. Microstructure of a W_p/Cu composite with the V_f ratio of 50:50 (the bright phase stands for tungsten) [34].

Fig. 21. Typical tensile stress-strain curves of W_p/Cu composites (tungsten V_f: 50 %) obtained at three test temperatures [34].

Fig. 22. Flat tile type composite target concept consisting of tungsten flat tile armor, W_p/Cu composite heat sink block and CuCrZr alloy (or W_f/Cu composite) cooling tube bonded to the composite via Cu interlayer.

Fig. 23. Test mock-up consisting of castellated tungsten tiles, CuCrZr alloy heat sink block with a cooling channel and functionally graded Wp/Cu composite interlayer between the armor and heat sink. The composite interlayer consisted of three layers (thickness: 1.5 mm for each) each with a different composition (Vf: 30, 50, 70 %), respectively [35].

Fig. 24 shows a micrograph of the metallographic section of the W_p/Cu composite interlayer after a HHF test at 20 MW/m² (3 cycles) [35].